Title	Low-frequency electrical conductivity of trabecular bone: Insights from in silico modeling
Author(s)	Cervantes, María José; Basiuk, Lucas O.; González-Suárez, Ana; Carlevaro, C. Manuel; Irastorza, Ramiro M.; María José Cervantes
Publication Date	2023-09-23
Publication Information	Cervantes, María José, Basiuk, Lucas O., González-Suárez, Ana, Carlevaro, C. Manuel, & Irastorza, Ramiro M. (2023). Low-Frequency Electrical Conductivity of Trabecular Bone: Insights from In Silico Modeling. Mathematics, 11(19), 4038. https://doi.org/10.3390/math11194038
Publisher	MDPI
Link to publisher's version	https://doi.org/10.3390/math11194038
Item record	http://hdl.handle.net/10379/18025
DOI	http://dx.doi.org/10.3390/math11194038

Article

Low-Frequency Electrical Conductivity of Trabecular Bone: Insights from In Silico Modeling

María José Cervantes [1,†], **Lucas O. Basiuk** [1,2,†], **Ana González-Suárez** [3,4], **C. Manuel Carlevaro** [1,2] **and Ramiro M. Irastorza** [1,2,*]

1   Instituto de Física de Líquidos y Sistemas Biológicos, CONICET La Plata, La Plata B1900BTE, Argentina; mjcervantes@iflysib.unlp.edu.ar (M.J.C.); lbasiuk@iflysib.unlp.edu.ar (L.O.B.); manuel@iflysib.unlp.edu.ar (C.M.C.)
2   Grupo de Materiales Granulares, Departamento de Ingeniería Mecánica, UTN FRLP, La Plata 1900, Argentina
3   Translational Medical Device Lab, School of Engineering, University of Galway, H91 TK33 Galway, Ireland; ana.gonzalezsuarez@universityofgalway.ie
4   Valencian International University, 46002 Valencia, Spain
*   Correspondence: rirastorza@iflysib.unlp.edu.ar
†   These authors contributed equally to this work.

Abstract: Background: The electrical conductivity of trabecular bone at 100 kHz has recently been reported as a good predictor of bone volume fraction. However, quantifying its relationship with free water (or physiological solution) content and the conductivities of its constituents is still difficult. Methods: In this contribution, in silico models inspired by microCT images of trabecular bovine samples were used to build realistic geometries. The finite element method was applied to solve the electrical problem and to robustly fit the conductivity of the constituents to the literature data. The obtained effective electrical conductivity was compared with the Bruggeman three-medium mixture model using a physiological solution, bone marrow and a bone matrix. Results: The values for the physiological solution plus bone marrow (together as one material) and the bone matrix that best captured the bone volume fraction in the two-medium finite element model were σ_{ps+bm} = 298.4 mS/m and σ_b = 21.0 mS/m, respectively. Additionally, relatively good results were obtained with the three-medium Bruggeman mixture model, with σ_{bm} = 103 mS/m, σ_b = 21.0 mS/m and σ_{ps} = 1200 mS/m. Simple linear relationships between the proportions of constituents depending on bone volume fraction were tested. Degree of anisotropy and fractal dimension do not show detectable changes in effective conductivity. Conclusions: These results provided some useful findings for simulation purposes. First, a higher value for the electrical conductivity of bone marrow has to be used in order to obtain similar values to those of experimental published data. Second, anisotropy is not detectable with conductivity measurements for small trabecular samples (5 mm cube). Finally, the simulations presented here showed relatively good fitting of the Bruggeman mixture model, which would potentially account for the free water content and could rescale the model for whole-bone electrical simulations.

Keywords: computer model; trabecular bone; electrical conductivity

1. Introduction

Bone health evaluation has been discussed for many years by scientists and clinicians, and there is a consensus that bone mineral density (obtained with the gold standard dual-energy x-ray absorptiometry) fails to predict certain types of bone fragility [1]. Trabecular bone architecture deterioration and microdamage are believed to be factors that increase fracture risk. They can be evaluated with peripheral quantitative computed tomography, but this is restricted to some parts of the body [2]. The mentioned techniques both involve

ionising radiation, so alternative methods are highly desirable. The dielectric properties (DP) of the tissue can be assessed non-invasively, for example by magnetic resonance [3]. The DP are attractive biophysical parameters for technological medical applications not only because of their non-ionising condition but also because of their low cost in measurement equipment. The DP of bone has been used and proposed for the following: evaluation of bone health [4], monitoring of bone healing [5] and bone growth stimulation [6,7]. Additionally, recent work on bone scaffolds considered electrical conductivity as a very important property that increases cellular response and improves osteogenic differentiation [8]. Therefore, tuning the electrical properties of scaffolds to mimic bone tissue properties (for example by using conductive polymers [9]) is a very promising approach. Despite these very recent developments and advances, there is still a lack of knowledge on how certain factors affect bone DP [10].

Bone is a hierarchical tissue and its structure is a complex matrix composed of several materials (collagen, water, minerals, marrow, etc. [11]) and structures (the macrostructure: trabecular or cancellous and cortical bone; the microstructure: Haversian systems, osteons, and single trabeculae, continuing to be the sub-microstructure, the nanostructure and the subnanostructure [12]). Most of these potential medical applications of DP imply numerical simulation of the electromagnetic problem [4,13–17]. Then, there is an interest in modeling and quantifying the influence of both composition and structure on the DP [10,11,18–20]. For example, Balmer et al. measured and modeled at the macro scale the correlation between bovine bone microstructure and electrical conductivity in the physiological state [10]. They concluded that a linear model considering two media (solid matrix and bone marrow) captures the microstructure (indirectly using the bone volume fraction, BV/TV). The authors proved that bone has a dominantly resistive behaviour and that any phase shift in the measurements are dominated by interface effects or due to stray capacitance. Consequently, for better interpretation, the authors recommended measuring at frequencies near 100 kHz, whose phase shift is almost zero. Sierpowska et al. studied the correlation between dielectric properties and several parameters of trabecular bone in the physiological state as well [21,22]. The authors concluded that the conductivity shows strong dependence on water content and that the interstitial bone marrow water has a major impact on overall trabecular bone conductivity. Additionally, they showed that fat and collagen content (the polarisation effects on its surface associated with the hydration layer) correlated only with the relative permittivity at frequencies higher than 100 kHz. According to these references, at the millimeter scale, it is valid to simplify modeling of the electric response of the trabecular bone using a two-medium material with its respective bone matrix conductivity (σ_b) and bone marrow conductivity (σ_{bm}). A simulation of such a material assumes that the conductivities of both components should be known, as should the material microstructure.

However, a computer simulation of the whole body electrical response (tenths/hundreds of centimeters) considering microstructural information is unaffordable. As an alternative, mixing theories from the effective medium theory has been used to homogenize the electrical properties of materials, which also allow for model rescaling [23]. Wei et al. proposed a dielectric model considering fat, water content and BV/TV in porcine non-physiological trabecular samples [18,19]. The authors proposed the unified mixing (UM) model [23] and obtained good results, which are unfortunately not applicable to in vivo conditions. Similar results using a three-medium Bruggeman mixture model were achieved by Ciuchi et al., but they only measured cortical porcine bone in the non-physiological state [20]. The authors considered hydroxyapatite crystals, the air and the environment; the material was collagen. Smith and Foster proposed the Maxwell mixture model for low-water-content tissues [24], and Kosterich et al. applied the same model to bone cortical tissue [25].

This paper focuses on the simulation of electrical conductivity of trabecular bone at 100 kHz and its relationship with its microstructure and free water. This frequency was selected in order to minimize interface and capacitance spurious effects, and consequently, the models were considered purely resistive. An in silico modeling approach was used,

in which computer models were developed to model the samples in a controlled way. The geometries were inspired by microtomography images of bovine trabecular bone samples. The obtained model intends to capture information about both the microstructure and water content by using mixed theory and finite element method (FEM) simulations. The objectives of this work are to estimate the conductivity values of the constituents of a two-medium model (bone matrix and bone marrow), to evaluate a simple three-medium Bruggeman mixture model for considering the free water content of the sample and to predict potential sources of measurement errors. The procedure to achieve this was validated with experimental published data of bovine samples in a physiological state. Once a confident model was obtained, the following problems were analysed: influence of the size of the sample and the anisotropy and influence of the washing process in sample preparation, which is related to the fat and water content of bone marrow.

2. Materials and Methods

2.1. Sample Preparation for Building Model Geometries

The models simulated in this paper were inspired by real geometries of bovine trabecular bone obtained using micro-computed tomography. Four cylindrical bovine trabecular bone samples (10 mm long, 16 mm diameter) were obtained from the femur head of two animals (A and B) from the local slaughterhouse within less than 24 h post-mortem (stored at 4 °C). The preparation process was already described in [26]; briefly, the samples were prepared using ad hoc tools: a handsaw made of two parallel blades and a hollow drill to extract cylinders. The marrow was removed from the samples in order to obtain good contrast in the micro-CT images. The process started with ultrasonication in a 2% tergazyme solution using a B-220 Ultrasonicator (Branson Ultrasonics Americas, Danbury, CT, USA) and then cleaning under a gentle flow of distilled water. Micro-CT of the samples was measured using a Bruker SkyScan 1173, and microstructure parameters were computed using BoneJ [27].

The bitmap files (obtained from the Bruker SkyScan software) of the four samples were edited in order to obtain several geometry models from a single sample (see Figure 1). We briefly describe the procedure; the high resolution images were down-sized by interpolation using anti-aliasing to avoid artifacts. After that, the region of interest (ROI) was then binarized (white and black, see Figure 2) using a threshold based on Otsu's method. A total of 43 geometries were built. The 3D geometries were built from the filtered micro-CT images using the 3D Slicer software [28]. Two types of geometry were simulated: cylinders ($\ell = 2.5$ mm and $r = 2.0$ mm, height and radius, respectively) and cubes ($\ell = 5$ mm), as shown in Figure 1B,D, respectively. The size of the cylindrical model was selected to study the effect of BV/TV without being affected by the anisotropy (see [10]), while the cubic model was the maximum possible size. Image processing and meshing were performed using scikit-image [29], Meshlab [30] and Gmsh [31].

2.2. Modeling and Computer Simulations

#### 2.2.1. Governing Equations and Boundary Conditions

The models were based on the electric problem, which was solved numerically using FEM implemented with FEniCS [32]. As the biological medium can be considered almost fully resistive at 100 kHz [10], the problem was approximated in its quasi-static form. Voltage Φ was computed using the following equation:

$$\nabla \cdot \sigma \nabla \Phi = 0 \qquad (1)$$

where σ is the conductivity of the materials (σ_b and σ_m, for bone matrix and marrow, respectively). Electric field vector $\mathbf{E}$ can be computed as $\mathbf{E} = -\nabla \Phi$. The power absorbed per unit tissue volume (also known as specific absorbed ratio (SAR)) can be calculated as $SAR = \sigma|\mathbf{E}|^2$. Then, it was integrated over the sample volume, obtaining the total power P [33]. For the boundary conditions, active and passive electrodes were set at voltages Φ_0

and 0 V, respectively (see Figure 1B). All the outer surfaces of the model (except those of the active and passive electrodes) were fixed to a null electric current. In order to obtain effective conductivity σ_{eff}, the power P was set equal to that obtained with a lumped resistor of length ℓ and area A (see Figure 1A). That is,

$$\sigma_{eff} = \frac{\ell P}{A \Phi_0^2}. \qquad (2)$$
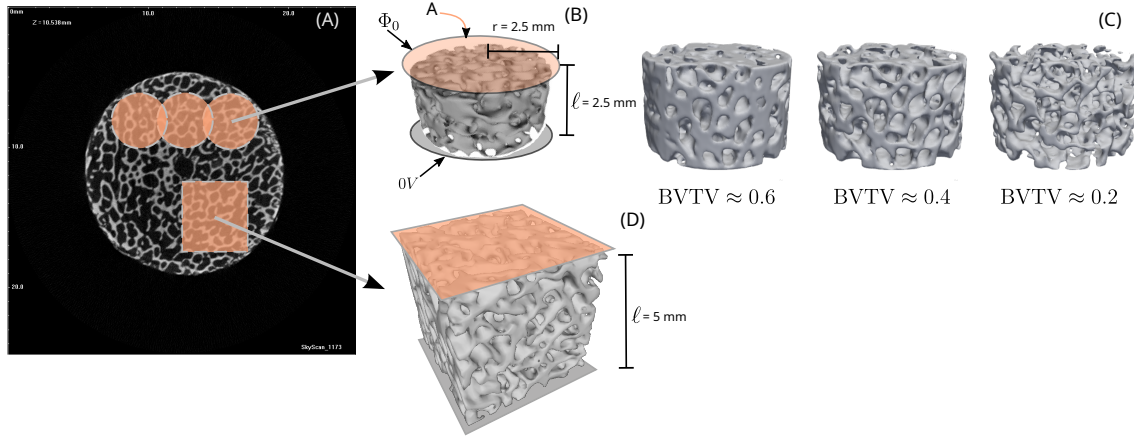
Figure 1. The model geometries. (**A**) MicroCT slice image. (**B**) Cylindrical sample (model 0) and (**C**) artificial procedure of trabeculae thinning to obtain the effective electrical conductivities. (**D**) Cubic sample to study the anisotropy effects.
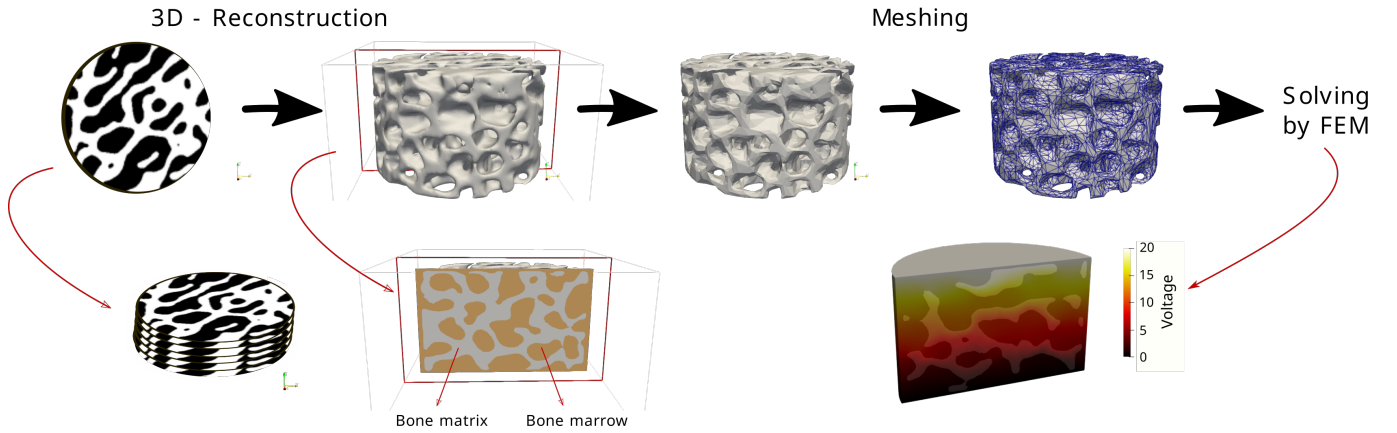
Figure 2. Schematic of the construction of in silico models and simulation process.

Figure 2 shows a visual representation of the in silico model construction process. Using the geometries obtained as described in Section 2.1, the finite element method was implemented using the continuous Galerkin method with Lagrange elements, using the consolidated open source software FEniCS [32] (an example of the code is available at https://github.com/rirastorza/RFA-tutorial, accessed on 1 August 2023). A mesh sensitivity analysis was performed using a selected sample, named model 0. Consecutive simulations were carried out in which the number of nodes was gradually increased and stopped when it was observed that the variation between the effective conductivities was less than 3%. The number of nodes was about 30,000. The execution time was about 20 s using a desktop computer Intel Core i7 CPU 2.93 GHz.

2.2.2. Estimation of Electrical Conductivities

One of the cylindrical geometries (model 0) was arbitrarily selected to obtain the conductivities of the constituent materials (σ_b and σ_{bm}). In order to obtain different BV/TV values (from 0.2 to 0.6), an artificial procedure of trabeculae thinning was applied (similar to that presented in [34]; see Figure 1C). Considering the BV/TV variable as independent, a series of simulations was carried out to minimize the difference between the obtained effective conductivity and the linear relationship proposed by Balmer et al. [10] ($\sigma_{\text{linear}} = 0.230 - 0.240 \cdot \text{BV/TV}$, in Sm^{-1}). We applied four numerical experiments in which one of the components was left free and the other was fixed. The minimisation process was performed using Brent's method with a Scipy routine [35]. Additionally, one numerical experiment was carried out leaving both conductivities as free parameters. In this case, the differential evolution optimisation method [36] was used. For validation of the results, the obtained conductivity values were used to simulate all the geometries ($n = 35$), and an absolute residue was computed for each case, using the following:

$$|\text{Residue}| = \sqrt{\sum_{i=1}^{n} \left(\sigma_{\text{linear}} - \hat{\sigma}_{eff} \right)^2} \tag{3}$$

2.2.3. Mixing Theory

Mixing theories are widely used in electromagnetics for homogenisation and model rescaling. The mixture formula proposed in this work is the effective Bruggeman model [23]. The most outstanding feature of Bruggeman formalism is that the considered phases are treated equally, which means that environment and inclusions have the same weight (the volume fraction). The complex relative permittivity ε^*_{eff} of a medium composed using N different materials is obtained with the following:

$$\sum_{j=1}^{N} f_j \frac{\varepsilon^*_j - \varepsilon^*_{eff}}{\varepsilon^*_j + 2\varepsilon^*_{eff}} = 0. \tag{4}$$

where f_j and $\varepsilon^*_j = \varepsilon'_j + \frac{\sigma_j}{i\omega\epsilon_0}$ are the proportion and the complex relative permittivity of the material j, respectively. It is important to mention that ε'_j and σ_j depend on the frequency, which is fixed at 100 kHz.

2.3. Tissue Characteristics

In this section, we review the literature values of the considered components of trabecular bone: bone matrix and bone marrow. All the reviewed values were taken from bovine bone samples (as long as they were available) measured at frequencies around 100 kHz.

Kameo et al. have developed a mechanical poroelastic model of a single trabeculae using a porosity of 0.05 (BV/TV = 0.95) [37]. Cortical bone is a porous material, with values of BV/TV from 0.92 to 0.94 [10,38]; therefore it is reasonable to simulate the bone matrix of the trabecular bone using the conductivity of cortical bone σ_{cb}. Balmer et al. obtained $\sigma_{cb} \approx 9.1$ mS m^{-1} [10]. A value one order of magnitude lower was obtained by Unal et al. [38] ($\sigma_{cb} \approx 0.2$ mS m^{-1}), but they used distilled water to clean the samples. The review of Amin et al. shows values from 6.6 to 20.8 mS m^{-1} [39].

Regarding bone marrow, it is known that it varies in cellular composition according to the age of the individuals. For a young individual, most of the marrow is red marrow, but for older individuals, the abundance of fat cells increases and the color of the marrow changes to yellow [40]. The results of Gabriel et al. show values from 20 mS m^{-1} to 100 mS m^{-1} (values extrapolated from figures) for pigs of 10 kg to 250 kg, and this can be explained by the water content (0.15 to 0.40, respectively). Samples of bone marrow from the femurs and tibiae of 1-month-old calves were measured in reference [24]. The volume fraction of water of the samples varied from 0.2 to 0.7, and the conductivities varied from

200 mS m^{-1} to 700 mS^{-1}, respectively (values obtained from figures). Finally, the results presented in the ITIS database are 3.82 mS^{-1} to 100 mS^{-1} [41,42].

It is important to note that free water hereafter will be indistinctly referred to as the physiological solution or porous water. We emphasize free water because we are interested in the water that can flow freely within pores [43].

3. Results

3.1. Microstructure Parameters

The cylindrical samples were used for studying the relationships between BV/TV and effective conductivity. The BV/TV mean (standard deviation) was 0.410 (0.07), with minimum and maximum values of 0.347 and 0.603, respectively. These samples were relatively smaller (2.5 mm) than the cubic samples (5 mm), and based on the reasoning of Balmer et al. [10], the importance of bone anisotropy increases when the bone region reaches an edge length of about 5 mm. In fact, the cube samples were used for evaluating anisotropy, and their results are summarized in Table 1. In addition to the BV/TV parameter, the degree of anisotropy (DA) and fractal dimenssion (FD) were computed with BoneJ software using the algorithms presented in [27].

Table 1. Microstructure properties of cubic samples.

| Sample	BV/TV	DA	FD
# 1 A	0.348	0.536	2.651
# 2 A	0.339	0.549	2.651
# 3 A	0.419	0.553	2.651
# 1 B	0.473	0.679	2.859
# 2 B	0.515	0.572	2.853
# 3 B	0.485	0.681	2.699
# 4 B	0.460	0.702	2.692
# 5 B	0.447	0.667	2.697

3.2. Estimation of Effective Electrical Conductivity Using FEM

The results of the general procedure described in Section 2.2.2 are summarized in Table 2. For example, in Simulation #1, the differential evolution algorithm searched by varying the σ_{bm} between 20 and 700 mS/m, while the matrix conductivity was fixed at $\sigma_b = 9.1$ mS/m.

Figure 3 shows the estimation of effective electrical conductivity using the results with minimum residues: Simulations # 1 and # 5. It should be noted that the estimation was performed with Sample 0 and that the validation was performed with Samples A and B.

Table 2. Simulation plan and results of two-medium model of cylindrical samples.

| Simulation | Range (mS/m) | | Results (mS/m) | | | |
	σ_{bm}	σ_b	σ_{bm}	σ_b	Residue	References
# 1	20–700	9.1	344.8	9.1	0.050	[10]
# 2	230	0.2–21	230.0	21.0	0.065	[10]
# 3	3.82 (yellow)	0.2–21	3.8	21.0	0.308	[42]
# 4	103 (red)	0.2–21	103.0	21.0	0.183	[42]
# 5	20–700	0.2–21	298.4	21.0	0.025	[24,42]
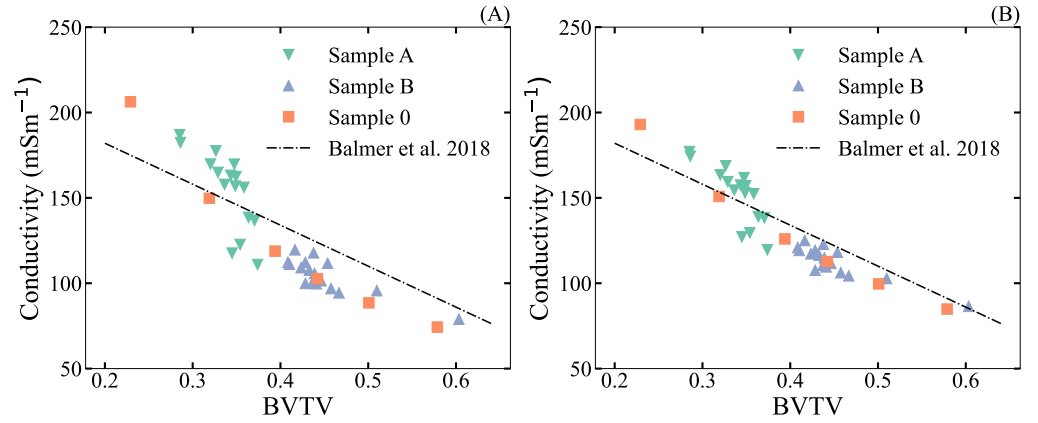
Figure 3. Results of estimating the effective electrical conductivity. Simulation of all samples using (**A**) Simulation # 1, fixing the conductivity of the bone matrix (**B**) Simulation # 5, varying both the conductivity of the bone matrix and the bone marrow.

3.3. Mixture Models

The values that best captured the BV/TV variable in the two-medium FEM model were σ_b = 21.0 mS/m and σ_{bm} = 298.4 mS/m. One question that arose is the amount of free water involved in the bone marrow value. We considered that no free water is inside the bone matrix (or its free water content is relatively constant). The simplest mixture model that can be tested is the Maxwell–Garnett model [23]. If we consider only the marrow, we have to achieve an effective conductivity of 298.4 mS/m. Taking for the physiological solution ε_1' = 78.0 and σ_1 = 1200 mS/m and for the bone marrow (without free water) the values from the database [41], then the proportions of water obtained were 0.97 and 0.49 for yellow and red marrow, respectively. These values are not consistent with those presented in the literature [43], which are around 20%. Therefore, another approach that can be evaluated is the Bruggeman model. The results presented next were computed using three materials ($N = 3$, in Equation (4)): physiological solution, bone matrix and bone marrow (without free water), $j = 1$, 2 and 3, respectively. Note that in Equation (4), the proportion, the relative permittivity and conductivity of each material are needed. The model tested was set as follows. The water proportion f_1 was defined as a variable, and the bone matrix proportion (f_2) was varied from 0.2 to 0.6, which was approximately the range of the BV/TV of the samples of this work and [10]. Once f_1 and f_2 were fixed, the other was determined: $f_3 = 1 - f_1 - f_2$. The values of the relative permittivity for the bone matrix and marrow (without water) were $\varepsilon_2' = 2.28 \times 10^2$ and $\varepsilon_3' = 1.73 \times 10^2$ (values from database [41]), respectively. Figure 4A shows the results when the values of conductivities were $\sigma_2 = 20.8$ mS/m and $\sigma_3 = 103$ mS/m. Two values for the proportion of free water were evaluated as 0.1 and 0.3. Figure 4B shows the result when the conductivities proposed by Balmer et al. [10] were used ($\sigma_2 = 9.1$ mS/m and $\sigma_3 = 230.0$ mS/m).

Figure 4 also shows the results of the Bruggeman model when the water content depends linearly on the BV/TV: $f_3 = A + Bf_2$; that is, the lower the BV/TV, the higher the water content. The reasoning followed to obtain A and B was to satisfy $f_2 = 0.2$, $f_3 = 0.3$ and $f_2 = 0.95$ (porosity of cortical bone [37]), and $f_3 = 0.05$ (free water content of cortical bone [44]).
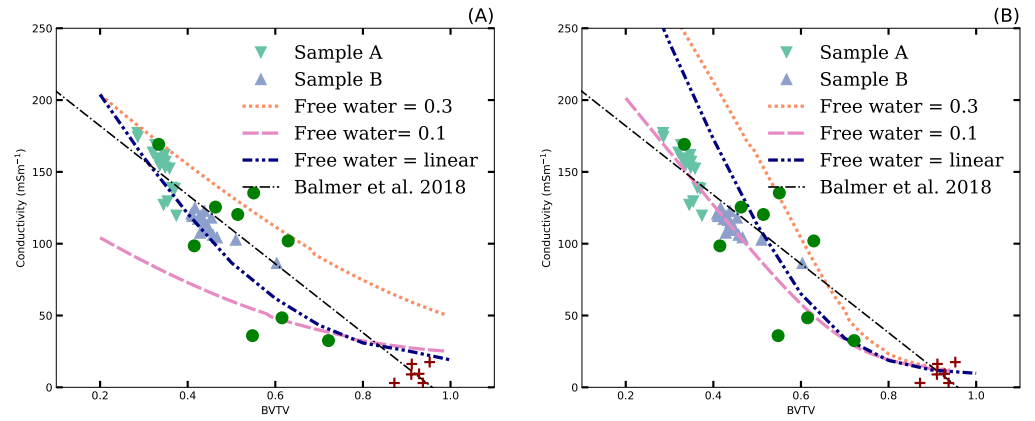
Figure 4. Results of mixture models (Bruggeman model with $N =3$ using two proportions of free water and a linear relationship between proportion of free water and BV/TV) compared with effective conductivity computed by simulation using FEM (same as Figure 3). The Balmer et al. linear relationship (dashed–dotted line) and experimental data (circle and +, trabecular and cortical) are also shown (data extracted from figures of [10]). (**A**) Values of reference [41] were used for porous and matrix (cortical bone and red marrow, respectively). (**B**) Values proposed by [10] were used.

3.4. Prediction of Potential Sources of Measurement Errors

3.4.1. Anisotropy

Cube geometries ($\ell = 5$ mm) were used in order to check whether the anisotropy can be detected by electrical measurements in such small samples. Figure 5A–C show the three types of simulation computed for each sample from Table 1. The results for these three simulations were three different effective conductivities. The ratios of the maximum and minimum values were computed and plotted against the degree of anisotropy and the fractal dimension (see Figure 5D,E). The minimum square linear estimation was plotted as a guide.
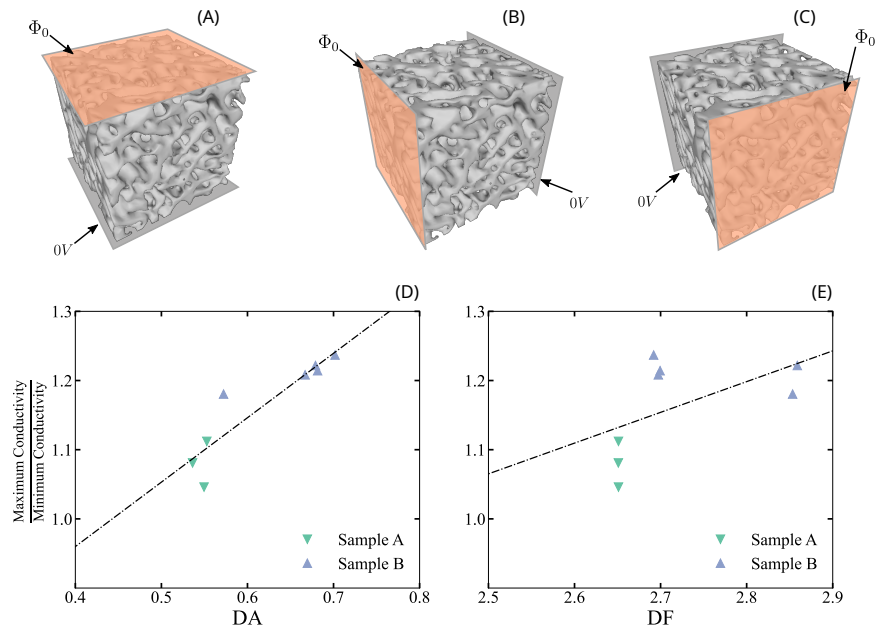
Figure 5. Study of anisotropy in cube samples. (**A**–**C**) show three measurement experiment models, where the same sample is measured in the three directions. (**D**,**E**) show the ratio of the maximum and minimum effective conductivity and the degree of anisotropy (DA), and the fractal dimension (FD), respectively.

A difference of 0.1 in degree of anisotropy resulted in approximately 10% of conductivity ratio, and this was the greatest difference detected in these models. No conclusive results were obtained with the fractal dimension.

3.4.2. Influence of Washing the Samples

Generally, during the cutting process, the samples are sprayed with a physiological solution (or similar) to prevent loss of moisture. Usually, after preparation, the samples are immersed in the physiological solution, frozen and finally thawed just prior to measurement. Saha and Williams warned that the electrical properties of cortical bone may be affected in the described process [45]. In this section, we simulated the diffusion of the physiological solution inside the porous space of the bone matrix. We selected the geometry of model 0, and the spatial distribution of the conductivity of the porous space was modeled with a Gaussian shape that smoothly goes from σ_{bm} = 298.4 mS/m (in the center of the sample) to σ_{ps}= 1200 mS/m (on the outer surface). The function when the sample was centered at the origin was as follows:

$$\sigma_{porous} = \sigma_{ps} - (\sigma_{ps} - \sigma_{bm}) \exp\left[-\frac{x^2 + y^2 + z^2}{2d^2}\right] \tag{5}$$

and with parameter d, we simulated a deeper diffusion inside the matrix. Figure 6 shows the results of 35 simulations varying parameter d from 0 to 5 mm. The percentage value of the conductivity with respect to the base value σ_{eff} (when d tends to infinity) is plotted in Figure 6B. Note that even with d = 4 mm, the overestimation of conductivity is 25% or greater.
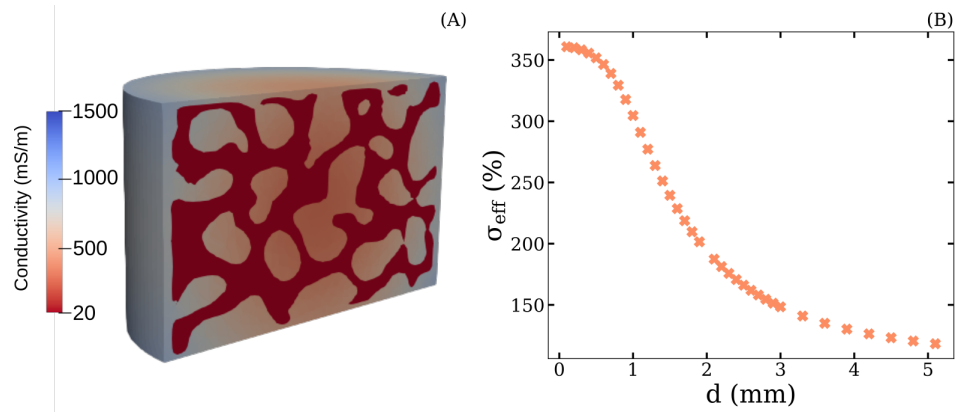
Figure 6. Physiological solution diffusion inside the porous bone matrix. (**A**) Example of the conductivity map in the 3D geometry; the conductivity of the porous space was defined with Equation (5). (**B**) Percent effective conductivity in function of parameter d.

4. Discussion

The results of this paper focused on the electrical conductivity of trabecular bone at 100 kHz. At this frequency, there is a consensus in the literature that bone can be considered a purely resistive medium because the phase shift is almost zero [10,19,22]. Considering this, we have studied the role of the microstructure and physiological solution (or free water that can flow within the pores) on the effective electrical conductivity of samples.

The experiments of Balmer et al. (at 100 kHz [10]) arrived at a linear relationship between BV/TV and the effective electrical conductivity of bone in a physiological state. These experiments were performed with samples of cortical and trabecular bone, with a mean BV/TV of 0.92 and 0.53, respectively. The authors also proposed values for the bone matrix and the bone marrow based on a simple two resistors in a parallel circuit, with $\sigma_{bm} \approx 230$ mS/m and $\sigma_b \approx 9.1$ mS/m, respectively. These values are different from those extensively used in the bibliography [42], $\sigma_{bm} = 103$ mS/m (red bone marrow),

$\sigma_{bm} = 3.82$ mS/m (yellow bone marrow) and $\sigma_b = 20.8$ mS/m. On the other hand, the compilation of Gabriel and coauthors indicates that the effective electrical conductivity of trabecular (cancellous) bone is around 83.9 mS/m, which makes some sense if the marrow is "red" but not when it is "yellow" (see the compiled information in [41]). Unfortunately, in this compilation, there is no information about the microstructure of the trabecular bone. In the computer results presented here, using realistic microstructure geometries, we obtained the values $\sigma_{bm} \approx 300$ mS/m and $\sigma_b \approx 21$ mS/m for marrow and matrix, respectively. These values were robustly validated using independent geometries. The bone matrix value agreed well with that presented by the Gabriel compilation for cortical bone but was double that of Balmer and coworkers. Regarding the bone marrow, a much higher value was obtained, which is more similar to the values presented by Smith and Foster [24]. These results show that, a simple model of two resistors in parallel [10] is not enough to capture BV/TV and both matrix and marrow electrical conductivities.

The reasoning commented above evidences that $\sigma_b \approx 21$ mS/m is a good enough value for bone matrix (at least for computer simulation considering microstructure), and hopefully, it can be considered relatively constant with the free water content. For bone marrow, the problem is more difficult, and the proportion of free water is not clearly known. Wei and collaborators measured the volume fraction of water in porcine trabecular bone by fitting a unified mixing dielectric model, but they obtained confusing results [19]. Instead of volume fraction, the authors considered mass fraction, arriving at mean values from 0.13 to 0.18, when the BV/TV was between 0.29 and 0.40. The work of Smith and Foster [24] considered the effective Maxwell mixture model and they measured volume fractions of water directly in the bone marrow, with values from 0.2 to 0.7. If BV/TV is around 0.4, then the bone marrow plus free water is $1 - 0.4 = 0.6$ and $0.6 \times 0.2 \approx 0.12$ and $0.6 \times 0.7 \approx 0.42$ for the lowest and highest values of volume fraction of water in bone marrow [24], respectively. The work of Sierpowska et al. has shown that at 100 kHz, the free water strongly affects the electrical conductivity of human trabecular bone and that it is mostly governed by the water inside the porous space [21], but no information about the water volume fraction was given. In conclusion, any value from 0.1 to 0.5 covers the range of the mentioned references for the water volume fraction. The results presented in this paper using the Bruggeman model are in line with a water volume fraction from 0.2 to 0.3 for trabecular bone. The best model for representing effective electrical conductivity of the cortical bone as well was obtained using the values of reference [41] (see Figure 4A). It should be noted that this is true when the free water volume fraction has a negative linear relationship with BV/TV (in Figure 4, the curve called "linear"), which can be interpreted as follows: the more porous the matrix, the more easily the free water flows into the matrix. Therefore, for a wide range, from 0.2 to 0.95 of BV/TV, and for a physiological solution content varying linearly with it from 0.05 to 0.3, we arrived at the following:

$$f_3 = 11/30 - f_2/3$$
$$f_1 = 1 - 11/30 - 2/3 f_2$$

(6)

where f_1 is the volume fraction of marrow, $f_2 =$ BV/TV and f_3 is the free water volume fraction. Consequently, the Bruggeman model using $\sigma_{bm} = 103$ mS/m, $\sigma_b = 21$ mS/m and $\sigma_{ps} = 1200$ mS/m for materials 1, 2 and 3, respectively, represented the effective electrical conductivity of bone (cortical and trabecular) at 100 kHz relatively well and can be a good candidate for simulation purposes. Logically, this is simplistic reasoning, and certain limitations should be mentioned, like the composition according to the age of the individuals. For a young individual, most of the marrow is red marrow, and more conductive (more free water) values are expected. On the other hand, for older individuals, the abundance of fat would give lower values of conductivity. Additionally, these values can be considered, for example, in the design of bone scaffolds in order to match not only the porosity of the developed matrix but also its electrical conductivity at that frequency. The idea of correcting the electrical attributes of the scaffolds in order to improve bone

healing by electrical stimulation is present in the literature but a deeper understanding of the native properties of bone are necessary [8,46].

Balmer et al. [10] commented that the importance of bone anisotropy increases when the bone region reaches an edge length of about 5 mm. To study this, we simulated cubic samples of this size, comparing the electrical conductivity with two parameters: degree of anisotropy and fractal dimension. We found no relevant information relating to the latter. Regarding the former, even differences between samples were captured by the variation in conductivity (which is around 10%), which certainly can be masked by measurement error. For example, Balmer and cohautors reported a root-mean-square (RMS) error of 31 mS/m for trabecular bone, which in 100 mS/m conductivity, represents 30%.

During washing and storing of the samples, the physiological solution could flow inside the pores of the bone matrix. Quantifying how this affects the electrical conductivity experimentally is very difficult. We intended to emulate it by varying the bone marrow conductivity with the coordinates: at the center of the sample, we assigned $\sigma_{bm} = 103$ mS/m, increasing to $\sigma_{ps} = 1200$ mS/m in a Gaussian shape until the border of the sample was reached. For example, if parameter d = 4 mm, at the border of the sample, a value of approximately 650 mS/m is reached, and the overestimation of the effective conductivity is around 25% (Figure 6B). Then, for dielectric property measurements, it is really important to carefully design a protocol to minimize the washing and storage time with the liquid phase of the physiological solution.

Limitations of the Study

The in silico model presented here has limitations regarding the assumptions of the material properties: (1) bone matrix and (2) bone marrow. The former is assumed to be isotropic, but it is known that even a single trabecula is anisotropic; in fact, several mechanical studies modeled the anisotropy due to collagen orientation using the finite element method [47,48]. As far as we know, the anisotropy of the dielectric properties of bone were explored only experimentally in macroscopic samples. As Ramos et al. mentioned, a study of anisotropy effects must be conducted [7]. The limitation related to bone marrow is that we consider it as a non-living medium; in fact, cells were not taken into account. Therefore, the results presented here should be interpreted carefully when in vivo application is simulated.

5. Conclusions

The low-frequency electrical conductivity of bone depends strongly on its microstructure and water content. The in silico 3D models at 100 kHz inspired by microCT images of bovine samples demonstrate two important things: First, a higher value of electrical conductivity of bone marrow has to be used in order to obtain similar values to those of experimental published data. Second, anisotropy is not detectable with conductivity measurements for small trabecular samples (5 mm cube). The simulations were also used to fit the Bruggeman mixture model, which would potentially enable us to account for the free water content and to rescale the model for whole-bone electrical simulations.

Author Contributions: Conceptualisation, A.G.-S., C.M.C. and R.M.I.; methodology, M.J.C. and L.O.B.; software R.M.I. and C.M.C.; formal analysis, A.G.-S.; writing—original draft preparation, M.J.C., L.O.B. and R.M.I.; writing—review and editing, A.G.-S. and C.M.C.; funding acquisition, R.M.I. and C.M.C. All authors have read and agreed to the published version of the manuscript.

Data Availability Statement: The data presented in this study are available on request from the corresponding author.

References

1. Ferretti, J.L.; Cointry, G.R.; Capozza, R.F.; Frost, H.M. Bone mass, bone strength, muscle–bone interactions, osteopenias and osteoporoses. *Mech. Ageing Dev.* **2003**, *124*, 269–279. [CrossRef]
2. Shi, X.; Liu, X.S.; Wang, X.; Guo, X.E.; Niebur, G.L. Effects of trabecular type and orientation on microdamage susceptibility in trabecular bone. *Bone* **2010**, *46*, 1260–1266. [CrossRef] [PubMed]
3. Katscher, U.; van den Berg, C.A. Electric properties tomography: Biochemical, physical and technical background, evaluation and clinical applications. *NMR Biomed.* **2017**, *30*, e3729. [CrossRef]
4. Kimel-Naor, S.; Abboud, S.; Arad, M. Parametric electrical impedance tomography for measuring bone mineral density in the pelvis using a computational model. *Med. Eng. Phys.* **2016**, *38*, 701–707. [CrossRef] [PubMed]
5. Lin, M.C.; Hu, D.; Marmor, M.; Herfat, S.T.; Bahney, C.S.; Maharbiz, M.M. Smart bone plates can monitor fracture healing. *Sci. Rep.* **2019**, *9*, 2122. [CrossRef] [PubMed]
6. Khalifeh, J.M.; Zohny, Z.; MacEwan, M.; Stephen, M.; Johnston, W.; Gamble, P.; Zeng, Y.; Yan, Y.; Ray, W.Z. Electrical stimulation and bone healing: A review of current technology and clinical applications. *IEEE Rev. Biomed. Eng.* **2018**, *11*, 217–232. [CrossRef]
7. Ramos, A.; Dos Santos, M.P.S. Capacitive stimulation-sensing system for instrumented bone implants: Finite element model to predict the electric stimuli delivered to the interface. *Comput. Biol. Med.* **2023**, *154*, 106542. [CrossRef]
8. Dixon, D.T.; Gomillion, C.T. Conductive scaffolds for bone tissue engineering: Current state and future outlook. *J. Funct. Biomater.* **2021**, *13*, 1. [CrossRef] [PubMed]
9. Balint, R.; Cassidy, N.J.; Cartmell, S.H. Conductive polymers: Towards a smart biomaterial for tissue engineering. *Acta Biomater.* **2014**, *10*, 2341–2353. [CrossRef]
10. Balmer, T.W.; Vesztergom, S.; Broekmann, P.; Stahel, A.; Büchler, P. Characterization of the electrical conductivity of bone and its correlation to osseous structure. *Sci. Rep.* **2018**, *8*, 8601. [CrossRef]
11. Sierpowska, J.; Lammi, M.; Hakulinen, M.; Jurvelin, J.; Lappalainen, R.; Töyräs, J. Effect of human trabecular bone composition on its electrical properties. *Med. Eng. Phys.* **2007**, *29*, 845–852. [CrossRef]
12. Rho, J.Y.; Kuhn-Spearing, L.; Zioupos, P. Mechanical properties and the hierarchical structure of bone. *Med. Eng. Phys.* **1998**, *20*, 92–102. [CrossRef] [PubMed]
13. Ron, A.; Abboud, S.; Arad, M. Home monitoring of bone density in the wrist—a parametric EIT computer modeling study. *Biomed. Phys. Eng. Express* **2016**, *2*, 035002. [CrossRef]
14. Wong, P.; George, S.; Tran, P.; Sue, A.; Carter, P.; Li, Q. Development and validation of a high-fidelity finite-element model of monopolar stimulation in the implanted guinea pig cochlea. *IEEE Trans. Biomed. Eng.* **2015**, *63*, 188–198. [CrossRef] [PubMed]
15. Zimmermann, U.; Ebner, C.; Su, Y.; Bender, T.; Bansod, Y.D.; Mittelmeier, W.; Bader, R.; van Rienen, U. Numerical simulation of electric field distribution around an instrumented total hip stem. *Appl. Sci.* **2021**, *11*, 6677. [CrossRef]
16. Feng, C.; Yao, J.; Wang, L.; Zhang, X.; Fan, Y. Idealized conductance: A new method to evaluate stiffness of trabecular bone. *Int. J. Numer. Methods Biomed. Eng.* **2021**, *37*, e3425. [CrossRef] [PubMed]
17. Blaszczyk, M.; Hackl, K. Multiscale modeling of cancellous bone considering full coupling of mechanical, electric and magnetic effects. *Biomech. Model. Mechanobiol.* **2022**, *21*, 163–187. [CrossRef]
18. Wei, W.; Shi, F.; Kolb, J. Impedimetric Analysis of Trabecular Bone Based on Cole and Linear Discriminant Analysis. *Front. Phys.* **2020**, *8*, 662. [CrossRef]
19. Wei, W.; Shi, F.; Zhuang, J.; Kolb, J.F. Comprehensive characterization of osseous tissues from impedance measurements by effective medium approximation. *AIP Adv.* **2021**, *11*, 105316. [CrossRef]
20. Ciuchi, I.V.; Olariu, C.S.; Mitoseriu, L. Determination of bone mineral volume fraction using impedance analysis and Bruggeman model. *Mater. Sci. Eng. B* **2013**, *178*, 1296–1302. [CrossRef]
21. Sierpowska, J.; Hakulinen, M.; Töyräs, J.; Day, J.; Weinans, H.; Kiviranta, I.; Jurvelin, J.; Lappalainen, R. Interrelationships between electrical properties and microstructure of human trabecular bone. *Phys. Med. Biol.* **2006**, *51*, 5289. [CrossRef]
22. Sierpowska, J.; Töyräs, J.; Hakulinen, M.; Saarakkala, S.; Jurvelin, J.; Lappalainen, R. Electrical and dielectric properties of bovine trabecular Bone—Relationships with mechanical properties and mineral density. *Phys. Med. Biol.* **2003**, *48*, 775. [CrossRef] [PubMed]
23. Sihvola, A.H. *Electromagnetic Mixing Formulas and Applications*; Number 47; The Institution of Engineering and Technology: London, UK, 1999.
24. Smith, S.R.; Foster, K.R. Dielectric properties of low-water-content tissues. *Phys. Med. Biol.* **1985**, *30*, 965. [CrossRef] [PubMed]
25. Kosterich, J.D.; Foster, K.R.; Pollack, S.R. Dielectric permittivity and electrical conductivity of fluid saturated bone. *IEEE Trans. Biomed. Eng.* **1983**, *30*, 81–86. [CrossRef] [PubMed]
26. Fajardo, J.E.; Carlevaro, C.M.; Vericat, F.; Berjano, E.; Irastorza, R.M. Effect of the trabecular bone microstructure on measuring its thermal conductivity: A computer modeling-based study. *J. Therm. Biol.* **2018**, *77*, 131–136. [CrossRef] [PubMed]

27. Domander, R.; Felder, A.; Doube, M. BoneJ2—Refactoring established research software. *Wellcome Open Res.* **2021**, *6*, 37. version 2. peer review: 3 approved. [CrossRef]

28. Fedorov, A.; Beichel, R.; Kalpathy-Cramer, J.; Finet, J.; Fillion-Robin, J.C.; Pujol, S.; Bauer, C.; Jennings, D.; Fennessy, F.; Sonka, M.; et al. 3D Slicer as an image computing platform for the Quantitative Imaging Network. *Magn. Reson. Imaging* **2012**, *30*, 1323–1341. [CrossRef]

29. van der Walt, S.; Schönberger, J.L.; Nunez-Iglesias, J.; Boulogne, F.; Warner, J.D.; Yager, N.; Gouillart, E.; Yu, T.; the scikit-image contributors. scikit-image: Image processing in Python. *PeerJ* **2014**, *2*, e453. [CrossRef]

30. Cignoni, P.; Callieri, M.; Corsini, M.; Dellepiane, M.; Ganovelli, F.; Ranzuglia, G. MeshLab: An Open-Source Mesh Processing Tool. In *Eurographics Italian Chapter Conference*; Scarano, V., Chiara, R.D., Erra, U., Eds.; The Eurographics Association: Lugano, Switzerland, 2008. [CrossRef]

31. Geuzaine, C.; Remacle, J.F. Gmsh: A 3-D finite element mesh generator with built-in pre-and post-processing facilities. *Int. J. Numer. Methods Eng.* **2009**, *79*, 1309–1331. [CrossRef]

32. Langtangen, H.P.; Logg, A. *Solving PDEs in Python*; Springer: Heidelberg, Germany, 2017. [CrossRef]

33. Irastorza, R.M.; Gonzalez-Suarez, A.; Pérez, J.J.; Berjano, E. Differences in applied electrical power between full thorax models and limited-domain models for RF cardiac ablation. *Int. J. Hyperth.* **2020**, *37*, 677–687. [CrossRef]

34. Irastorza, R.M.; Blangino, E.; Carlevaro, C.M.; Vericat, F. Modeling of the dielectric properties of trabecular bone samples at microwave frequency. *Med. Biol. Eng. Comput.* **2014**, *52*, 439–447. [CrossRef]

35. Virtanen, P.; Gommers, R.; Oliphant, T.E.; Haberland, M.; Reddy, T.; Cournapeau, D.; Burovski, E.; Peterson, P.; Weckesser, W.; Bright, J.; et al. SciPy 1.0: Fundamental Algorithms for Scientific Computing in Python. *Nat. Methods* **2020**, *17*, 261–272. [CrossRef]

36. Storn, R.; Price, K. Differential evolution–a simple and efficient heuristic for global optimization over continuous spaces. *J. Glob. Optim.* **1997**, *11*, 341–359. [CrossRef]

37. Kameo, Y.; Ootao, Y.; Ishihara, M. Poroelastic analysis of interstitial fluid flow in a single lamellar trabecula subjected to cyclic loading. *Biomech. Model. Mechanobiol.* **2016**, *15*, 361–370. [CrossRef] [PubMed]

38. Unal, M.; Cingoz, F.; Bagcioglu, C.; Sozer, Y.; Akkus, O. Interrelationships between electrical, mechanical and hydration properties of cortical bone. *J. Mech. Behav. Biomed. Mater.* **2018**, *77*, 12–23. [CrossRef]

39. Amin, B.; Elahi, M.A.; Shahzad, A.; Porter, E.; O'Halloran, M. A review of the dielectric properties of the bone for low frequency medical technologies. *Biomed. Phys. Eng. Express* **2019**, *5*, 022001. [CrossRef] [PubMed]

40. Gabriel, C.; Peyman, A. Dielectric properties of biological tissues; variation with age. *Conn's Handb. Models Hum. Aging* **2018**, 939–952. [CrossRef]

41. Hasgall, P.; Di Gennaro, F.; Baumgartner, C.; Neufeld, E.; Gosselin, M.; Payne, D.; Klingenböck, A.; Kuster, N. *It'is Database for Thermal and Electromagnetic Parameters of Biological Tissues*, Version 3.0; 2015. Available online: https://itis.swiss/virtual-population/tissue-properties/downloads/database-v4-1/ (accessed on 1 March 2023).

42. Gabriel, C. *Compilation of the Dielectric Properties of Body Tissues at RF and Microwave Frequencies*; Technical Report; King's Coll London (United Kingdom) Dept. of Physics: London, UK, 1996.

43. Surowiec, R.K.; Allen, M.R.; Wallace, J.M. Bone hydration: How we can evaluate it, what it can tell us, and is it an effective therapeutic target? *Bone Rep.* **2022**, *16*, 101161. [CrossRef]

44. Abbasi-Rad, S.; Akbari, A.; Malekzadeh, M.; Shahgholi, M.; Arabalibeik, H.; Rad, H.S. Quantifying cortical bone free water using short echo time (STE-MRI) at 1.5 T. *Magn. Reson. Imaging* **2020**, *71*, 17–24. [CrossRef]

45. Saha, S.; Williams, P. Effect of various storage methods on the dielectric properties of compact bone. *Med. Biol. Eng. Comput.* **1988**, *26*, 199–202. [CrossRef]

46. Saberi, A.; Jabbari, F.; Zarrintaj, P.; Saeb, M.R.; Mozafari, M. Electrically conductive materials: Opportunities and challenges in tissue engineering. *Biomolecules* **2019**, *9*, 448. [CrossRef] [PubMed]

47. Hammond, M.A.; Wallace, J.M.; Allen, M.R.; Siegmund, T. Incorporating tissue anisotropy and heterogeneity in finite element models of trabecular bone altered predicted local stress distributions. *Biomech. Model. Mechanobiol.* **2018**, *17*, 605–614. [CrossRef] [PubMed]

48. Wang, Y.; Ural, A. A finite element study evaluating the influence of mineralization distribution and content on the tensile mechanical response of mineralized collagen fibril networks. *J. Mech. Behav. Biomed. Mater.* **2019**, *100*, 103361. [CrossRef] [PubMed]